Iron rich glauconite sand as an efficient phosphate immobilising agent in river sediments

Lei Xia [a,*], Tom David [a], Mieke Verbeeck [b], Yaana Bruneel [c], Erik Smolders [a]

[a] Division of Soil and Water Management, Department of Earth and Environmental Sciences, KU Leuven, Kasteelpark Arenberg 20 bus 2459, 3001 Leuven, Belgium.

[b] Rothamsted Research, Sustainable Agriculture Sciences, North Wyke, EX20 2SB, UK.

[c] Laboratoire de Mesure et Modélisation de la Migration des Radionucléides (L3MR), CEA Commissariat à l'énergie atomique et aux énergies alternatives, Paris-Saclay, France

*Corresponding author: E-mail: lei.xia@kuleuven.be

Abstract

The reductive dissolution of iron (Fe) (oxy)hydroxides in sediments releases phosphorus (P) to the overlying water and may lead to eutrophication. Glauconite sands (GS) are rich in Fe and may be used as readily available P sorbents. This study was set up to test effects of dose and type of GS on the P immobilisation in sediments under hypoxic conditions. Three different GS were amended to a P-rich river sediment at doses of 0% (control), 5% and 10% (weight fractions) and incubated with overlying water in batch laboratory conditions. Glutamate was added to the solution after 15 days to deplete any residual dissolved oxygen from the sediment-water interface. In the first 15 days, the P concentration in the overlying water peaked to 1.5 mg P L^{-1} at day 9 in the control and decreased to 0.9 mg P L^{-1} at lowest Fe-dose and to 0.03 mg P L^{-1} at the highest Fe-dose, the effects of GS type and dose were explained by the Fe dose. After 15 days, the added glutamate induced a second, and larger peak of P in the overlying water in sediment, that peak was lower in amended sediments but no GS dose or type related effects were found. This suggests that freshly precipitated P species at the sediment-water interface can be remobilised. This study highlights the potential for using this natural mineral as a cheap and easily available sediment remediation material, but its longevity under rare extreme conditions needs to be further investigated.

Keywords: Phosphorus release; Iron-rich glauconite sand; Amendment; Sediment-water interactions; Eutrophication

1. Introduction

Eutrophication has become a worldwide environmental problem due to excessive discharge of nutrients into water systems. It promotes the growth of algae and cyanobacteria and diminishes the ecological and economic value of freshwaters. Phosphorus (P) has been identified as one of the key factors responsible for eutrophication, thus constraining P concentration in surface waters is vital to mitigate eutrophication. The lowland river system of the Flemish region in Belgium suffers from high P concentrations during summer periods. The soluble reactive P (SRP) concentration is, on average, a factor 2.8 higher in summer than in winter (Smolders et al., 2017). This seasonality in P concentrations is explained by internal P loading due to reductive dissolution of ferric iron (Fe(III)) (oxy)hydroxides that are strong sorbents for phosphate (PO_4). During summer low flow periods, high sediment respiration and low dissolved oxygen (DO) resupply lead to hypoxia at the sediment-water interface (SWI) (van Dael et al., 2020b). Then Fe(III) (oxy)hydroxides are reduced to Fe(II), resulting in the subsequent P release from sediment. Therefore, it is urgent to explore an effective method to reduce internal P loading.

Geo-engineering sediments by dosing immobilising agents to alter P biogeochemical cycles has become an attractive tool to target the internal P loading (Spears et al., 2014). Many P immobilising agents have been explored for lakes, including aluminium (Al) salts (Huser et al., 2016; Jensen et al., 2015), Al-modified materials (Gibbs et al., 2011; Wang et al., 2019), Fe salts and Fe rich materials (Wang et al., 2013a, 2021), lanthanum (La) modified clay minerals (Copetti et al., 2015), and calcium (Ca) rich materials (Yin et al., 2013). Among them, Fe rich P sorbents have been used to reduce P in surface waters for decades due to their high affinity towards PO_4, their low cost and ubiquity (Wang et al., 2021). The Fe rich sorbents can effectively immobilise P in sediment under oxic conditions through adsorption and/or precipitation (Liu et al., 2017; Mucci et al., 2018; Zou et al., 2017). However, under anoxic conditions, the Fe rich sorbents often lose their binding capacity due to reduction of Fe(III) to Fe(II) (Kleeberg et al., 2013) that dissolves and releases P. The P released can be trapped by residual Fe(III)(oxy)hydroxides through adsorption or co-precipitation (Smolders et al., 2017) and/or precipitate with reduced Fe(II) as vivianite $(Fe(II)_3\ (PO_4)_2 \bullet 8$

H_2O) (Heinrich et al., 2021; Voegelin et al., 2013). Therefore, the redox sensitivity of Fe rich sorbents will not impede their P immobilisation ability as long as the reactive Fe(III) exceeds the capacity of reduction.

Glauconite sands (GS) are one of the widely available Fe rich sands. The mineral glauconite is a Fe potassium (K) phyllosilicate, mainly present as course pellets in the silt and sand fraction (0.002-2 mm). The structure of this mineral is similar to Fe rich illite, a typical three-layer phyllosilicate consisting of two silicon oxygen tetrahedrons and an alumina oxygen octahedral (T:O:T layer) (Bruneel et al., 2020; Chen et al., 2016). The GS of Diest formations contain high Fe, with average total Fe content of 16-23.5% and a typical Fe(III)/Fe(II) ratio of 9/1 (Bruneel et al., 2020). Under variable redox conditions the structural Fe can be oxidized/reduced by electron transfer in the crystal structure and part of the Fe can be released from the structure. The Fe released can precipitate as a coating on the glauconite or quartz grains (Fig. S1). These Fe coatings can be extracted with acid ammonium oxalate (i.e. reactive Fe), ranging between 0.6% and 0.9% of GS (Bruneel et al., 2021, 2020). The presence of Fe (oxy)hydroxides makes these GS potentially suitable as solid P sorbents. In our previous work, the immobilisation efficiency of GS as sediment amendment was tested in a dynamic flume system under hypoxic conditions. It illustrated that GS amendment reduced P release from sediment to the overlying water, with three times lower SRP concentration in GS amended treatments than in unamended treatments at a dose of 10% by weight of total sediment (Van Dael et al., 2021). The single GS treatment showed an excellent P immobilisation efficiency, while it was still unclear how the dose and the properties of GS affected its efficiency.

In this study the effects of dose and types of GS were investigated to obtain the optimal P immobilisation efficiency after GS amending to P rich river sediment. It is speculated that the reactive Fe and Al in the GS, i.e., the acid ammonium oxalate extractable elements, indicates the effective P immobilisation capacity of the amendment. That reactive Fe might, however, not be efficient under strict anaerobic conditions when most Fe is reduced, unless Fe(II) may scavenge P through vivianite precipitation and/or Fe(II) oxidation at the SWI. The P adsorption capacity of GS was measured under aerobic conditions, and it was tested if that capacity, or its affinity, indicate P immobilisation better than reactive Fe and Al. A full factorial batch

incubation was set up with three different types of GS and two doses. The sediment was incubated for 15 days under natural conditions with the amendments followed by the addition of glutamate (GLU) to the solution to deplete any residual DO from SWI. The treatment effects on the peaks of soluble reactive P were used to test the hypotheses.

2. Materials and methods

2.1 Sediment and GS characterisation

The sediment was sampled from Devebeek in Pittem, Flanders (50°58'50.5 "N, 3°16'29.3 "E). This sediment was chosen due to its large molar P/Fe ratio and the high P concentrations in the stream, i.e., the long-term average total dissolved P (TDP) concentration in that river was 1.4 mg P L^{-1}, well exceeding the environmental standard of 0.1 mg P L^{-1} (van Dael et al., 2020a). In total, 10 L of sediment was collected from the top 5 cm sediment layer by using a shovel and was stored at 4 °C. Then, the sediment was homogenized, sieved over 6.3 mm to remove gravel and undecomposed organic debris. A sub-sample of sediment was dried, sieved (2 mm) and extracted with 0.2 M acid ammonium oxalate (pH=3) in the dark at a solution-solid ratio of 50 L kg^{-1} under 2 h of shaking, to determine the content of poorly crystalline Fe, Al, and manganese (Mn) oxyhydroxides and the associated P (Schwertmann, 1964). The oxalate method extracts reactive Fe and Al, which have a high affinity for PO_4 (Wang et al., 2013c).

Three natural Fe rich GS with contrasting properties were collected in Lubbeek, Belgium (50°53'06.4"N 4°46'08.9"E). The GS was present as weathered (oxidised) outcroppings of the Diest formation in the Hageland region and were referred to GS1, GS2 and GS3. These GS had a glauconite content of 43-50% (Bruneel et al., 2021). The reactive content of Fe and Al in GS samples were determined after acid ammonium oxalate extractions by Inductively Coupled Plasma Optical Emission Spectrometry (ICP-OES, iCAP 7000 series). In addition, the total content of Fe, Al and P in the GS were determined after aqua regia digestion by Inductively Coupled Plasma Mass Spectroscopy (ICP-MS, Agilent 7700x, Agilent Technologies).

2.2 Phosphate adsorption experiment

The PO_4 adsorption experiment on the GS was carried out in aerobic conditions under batch mode to quantify the P sorption capacity of three GS. One gram (air-dried) of three GS was added into 40 mL centrifuge tubes with 20 mL of various P solutions in 10 mM $CaCl_2$ (0-200 mg P L^{-1}), the pH of the initial P solution was ranging from 6.6 to 7.4. The 10 mM $CaCl_2$ solution was used to mimic the ionic strength of the sediment solution. The tubes were placed on an end-over-end shaker (20 ℃) for 24 h at 30 rpm. The solutions were then centrifuged and the supernatants were filtered through a 0.45 µm membrane. The initial and final SRP concentrations were determined by molybdenum blue method (Murphy and Riley, 1962).

2.3 Sediment amendment and incubation

The effect of GS amendment to the sediment on P dynamics from the sediment to the overlying water was studied in a batch laboratory incubation experiment. A mixture between the sediment and three types of GS were incubated at two GS doses, i.e., 5% and 10% (dry weight of total sediment, equivalent to 1.6 and 3.2 kg m^2, respectively), including an unamended control. The added amount of GS was based on our previous study (Van Dael et al., 2021). All the treatments were duplicated in a full factorial design except the control that was triplicated (n = 15). For the control, the homogenized sediment was added into 1.1 L polypropylene pots (diameter 9.5 cm) to a height of 5 cm (211 g dry sediment). For the GS treatments, the homogenized sediment was firstly added to a height of 4 cm, then the mixture of sediment and GS (11 g or 21 g) was added on top of this sediment. Next, 650 mL of 10 mM $CaCl_2$ solution was gently added to each pot. The pots were closed and incubated in darkness at 20 ℃ for 28 days. Sodium glutamate (GLU, 31 mg C L^{-1} overlying water) was added to each pot at day 15 to develop a high biological oxygen demand environment (BOD, dose is equivalent to 50 mg O_2 L^{-1}), to mimic the situation during the summer period.

During the experiment, 5 mL overlying water was taken at 1 cm above the SWI with a pipette without prior mixing, this sampling was made periodically between 1-28 days. The solution was filtered (0.45 µm) and analysed for SRP using the molybdenum blue method. A sub-sample was acidified (1% HNO_3) and

analysed for major elements (Fe, Mn) using ICP-MS. The 5 mL of overlying water removed during each sampling time was not replenished with fresh $CaCl_2$.

Sediment probes (3.5 cm × 17 cm, Fig. S2) of diffusive equilibration in thin film (DET) and diffusive gradient in thin films (DGT) were vertically deployed at day 22 to investigate the P flux across the SWI under hypoxic conditions. The DET and DGT probes measure vertical profiles of soluble concentration of solutes in pore water (DET) and labile concentrations (DGT) in sediment. The DET and DGT probes were bubbled with N_2 before deployment. Then one deoxygenated DET and DGT probe was deployed in one of control and 10% GS treatments (4 DET and 4 DGT probes in total) for 24 h. The DET probe was prepared according to the procedure described by Baken et al. (2015), consisting of a polyacrylamide diffusive gel and a 0.45 μm nitrocellulose membrane filter (Amersham™ Protran®, Merck). During deployment, solutes equilibrate with diffusive gel and the concentration in the DET gel will be equal to that in sediment pore water (Davison et al., 1991). The DGT probe was prepared according to Guan et al. (2015), consisting of a zero sink binding layer (Zr-oxide gel), a polyacrylamide diffusive gel, and a 0.45 μm nitrocellulose membrane filter. After 24 h deployment, the probes were dismantled, the diffusive gels in DET and binding gels in DGT were cut into slices of 3 mm × 18 mm. The DET gels were eluted in 1 mL of 1 M HCl for at least 24 h, then the elution liquid was diluted and measured for P and Fe by using ICP-MS. The DGT gels were eluted in 1 mL of 0.5 M NaOH for at least 24 h and the elution was measured for P by using molybdenum blue method.

The pH and dissolved oxygen (DO) profiles of the overlying water were measured at day 22 before the probe deployment. The pH was measured at 1 cm above the SWI using a pH meter (Metrohm, Belgium). The DO profile was measured on one replicate of all treatments (n=7) using an O_2 micro sensor (tip diameter 100 μm; Unisense, Denmark) mounted on a motor-driven micromanipulator. To further investigate the changes in reactive Fe content and molar P/Fe ratio in amended and unamended sediments after incubation, sediment samples from the top layer (to 1 cm) and from subsurface (below 1 cm) were extracted with acid ammonium oxalate and analysed for Fe and P using ICP-OES.

2.4 Data analysis

The degree of phosphorus saturation (DPS) is calculated by Eq. (1).

$$DPS = \frac{P_{ox}}{0.5\ (Fe_{ox}+Al_{ox})} \times 100\% \quad \text{(Eq. 1)}$$

where P_{ox}, Fe_{ox} and Al_{ox} are oxalate extractable P, Fe and Al in sediment or in GS (mmol kg^{-1}).

The P adsorption capacity of the three GS was assessed by fitting the experimental data with Langmuir model adsorption isotherm. The Langmuir isotherm model is defined by Eq. (2).

$$Q_e = \frac{Q_{max}\, K_L C_e}{1+ K_L C_e} \quad \text{(Eq. 2)}$$

where Q_e is the amount of P adsorbed on GS (mg P kg^{-1} GS); C_e is the measured SRP concentration after 24 h (mg L^{-1}); Q_{max} is the maximum SRP adsorption capacity (mg P kg^{-1} GS); K_L is the Langmuir adsorption constant (L mg^{-1}).

The molar ratio of P and Fe in the sediment surface (1 cm) after GS amendment can be calculated by Eq. (3).

$$\frac{P}{Fe} = \frac{W_1 P_{ox1}+W_2 P_{ox2}}{W_1 Fe_{ox1}+W_2 Fe_{ox2}} \quad \text{(Eq. 3)}$$

where W_1 is the mass of dry sediment in 1 cm depth (g); W_2 is the mass of GS added to the sediment (g); P_{ox1} and Fe_{ox1} are the oxalate extractable P and Fe in the sediment (mmol g^{-1}); P_{ox2} and Fe_{ox2} are the oxalate extractable P and Fe in the GS (mmol g^{-1}).

The DGT labile P concentration (C_{DGT}, mg L^{-1}) is calculated by Eq. (4) and Eq. (5).

$$M = \frac{C_e(V_g+V_e)}{f_e} \quad \text{(Eq. 4)}$$

$$C_{DGT} = \frac{M\Delta g}{DAt} \quad \text{(Eq. 5)}$$

where *M* is the total mass of P bound to the binding layer during the contact with sediment (mg); C_e is the P concentration in the elution (mg L^{-1}); V_g and V_e are the volume of the binding gel (0.00002 L) and the

elution solution (0.001 L); f_e is the elution factor (0.95); Δg is the thickness of the diffusive layer (diffusive gel and filter membrane, 0.052 cm); *D* is the diffusion coefficient (5.27×10^{-6} cm^2 s^{-1} at 20℃); *A* is the contact area of the 0.3 cm DGT (0.54 cm^2); *t* (s) is the contact time between the DGT and the sediment.

The P immobilisation efficiency (*IE*, %) by GS amendment is calculated by Eq. (6).

$$IE = \frac{C_1 - C_2}{C_1} \times 100 \quad \text{(Eq. 6)}$$

where C_1 (mg L^{-1}) is the SRP concentration at the moment when SRP peaked in the control sediment and C_2 is the corresponding SRP concentration in the GS treated sediment.

Statistical analyses were performed using the JMP® Pro version 14.0.0. To test the treatment effects, peak concentrations of SRP and Fe were selected (day 9 and day 22, see Fig. 2). Differences in SRP and Fe concentrations, the pH of the overlying water and the molar P/Fe of the surface and bulk sediment between treatments and control were identified with the Dunnett's test. A two-way ANOVA was used to test the effect of GS type, GS dose and their interaction on peak SRP and Fe concentrations, the data in the control was excluded. A general linear regression model with depth added as a random factor was used to analyse the treatment effects on P (both DET and DGT) and Fe (only DET) in the sediment pore water. Pearson's correlation coefficients were calculated to analyse which GS properties determine P immobilisation efficiency and Fe release, and the control data were not included except for the calculation of the P immobilisation efficiency with Eq. 5.

3. Results

3.1 Sediment and GS Characteristics

The molar P/Fe ratio in the sediment was 0.32 (Table 1), exceeding the 0.12 limit above which internal loading of P becomes pronounced in rivers (Smolders et al., 2017). A large fraction of the total Fe in GS (more than 95%) was not oxalate extractable Fe (Fe_{ox}, Table 1), indicating that most Fe in the GS is present in the phyllosilicate structure of glauconite. The three GS differed by a factor of 10 in Fe_{ox} concentration, while they differed by a factor of 4 in degree of P saturation (DPS). After amending the sediment with GS,

the theoretical molar P/Fe ratio of the top 1 cm layer remained 0.32 for GS1 amended sediment (both doses), decreased to 0.29 and 0.26 for GS2 amended sediment (5 and 10% dose, respectively) and to 0.28 and 0.25 for GS3 amended sediment (Table S1).

The P adsorption isotherms to the GS in aerobic conditions showed that GS3 has the highest maximum adsorption capacity (Q_{max}), while GS1 and GS2 had about twofold lower P adsorption capacity (Fig. 1 and Table 1). That Q_{max} is, surprisingly, not proportional to the molar sum of (Fe_{ox}+Al_{ox}), i.e., GS2 has similar Q_{max} as GS1 although the molar sum of (Fe_{ox}+Al_{ox}) in GS2 is a factor of 3 higher than that of GS1. However, the GS2 has the largest K_L and the isotherms show that the P adsorption at low (and relevant, i.e., < 10 mg P L^{-1}, Funes et al., 2018; Lyngsie et al., 2014) SRP concentrations is about in proportion to the molar sum of (Fe_{ox}+Al_{ox}), i.e., GS3 > GS2 > GS1. In addition, despite that all GS contained P, none of GS released SRP (Table 1).

Table 1. Characteristics of sediment and glauconite sands (GS), the parameters and the R^2 of the Langmuir model were fitted to a phosphate adsorption isotherm (Eq. 2).

	Sediment	**GS1**	**GS2**	**GS3**
Fe_{ox} (mg kg^{-1})[a]	6500 ± 110	470 ± 30	3400 ± 230	4500 ± 340
Al_{ox} (mg kg^{-1})[a]	380 ± 3	450 ± 14	370 ± 4	750 ± 30
Mn_{ox} (mg kg^{-1})[a]	220 ± 4	42 ± 7	14 ± 4	220 ± 45
P_{ox} (mg kg^{-1})[a]	1200 ± 21	50 ± 2	30 ± 1	100 ± 10
DPS (%)[b]	57 ± 1	13 ± 0.5	3 ± 0.2	6 ± 0.2
P/Fe (mol mol^{-1})[c]	0.32 ± 0.004	0.19 ± 0.01	0.02 ± 0.001	0.04 ± 0.001
Total Fe (g kg^{-1})[d]	n.a	80 ± 8	80 ± 5	210 ± 16
Total Al (g kg^{-1})[d]	n.a	12 ± 1	11 ± 1	25 ± 2
Total Mn (mg kg^{-1})[d]	n.a	70 ± 5	30 ± 3	200 ± 5
Total P (mg kg^{-1})[d]	n.a	520 ± 76	440 ± 47	1800 ± 42

Q_{max} (mg P kg^{-1})[e]	n.a	650 ± 50	590 ± 20	1230 ± 70
K_L (L mg^{-1})[e]	n.a	0.06 ± 0.02	0.52 ± 0.26	0.16 ± 0.07
SRP release (mg L^{-1})	n.a	<LOQ	<LOQ	<LOQ
R^2	n.a	0.82	0.89	0.94

[a] Ammonium oxalate extraction (pH=3) in solution-solid ratio of 50 L kg^{-1}. [b] the degree of P saturation (DPS). [c] Molar ratio of oxalate extractable P and Fe in sediment and in the GS. [d] Aqua regia digestion. [e] The maximum P sorption capacity (Q_{max}) and Langmuir constant (K_L) obtained from the P adsorption isotherm. < LOQ = below the level of quantification (0.01 mg L^{-1}). n.a. = not available.

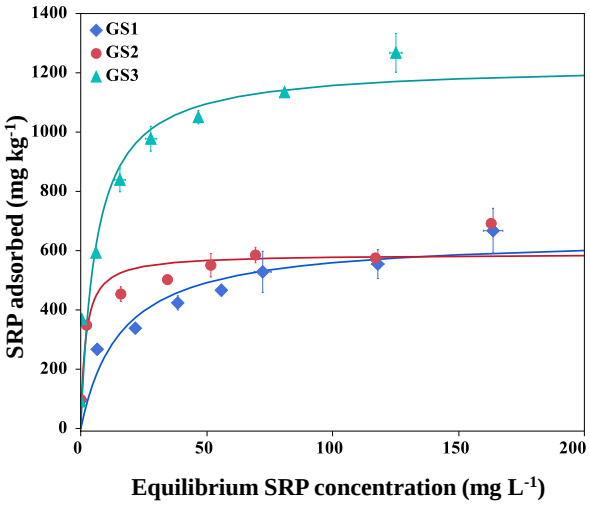

Fig. 1. Adsorption isotherm of soluble reactive P (SRP) on three GS. Symbols represent experimental results, lines the fitted Langmuir model. Error bars denote standard error of the means (n = 2).

3.2 The effect of GS amendment and GLU addition on P release

The first phase in the incubation without GLU addition yielded a significant dose and GS type dependent effect on SRP concentrations in the overlying water (Fig. 2). In the control, the SRP concentration increased from < 0.009 mg L^{-1} (detection limit) to 1.5 mg L^{-1} over 9 days, then followed by a decrease. The addition of GS succeeded in decreasing the SRP peak, thus the SRP peak concentrations were likely more relevant and selected for statistical analysis. At the 5% dose, only GS3 significantly reduced the P peak at day 9 by a factor of 3.4 compared to the control (Dunnett's test, $p < 0.005$), at the 10% dose, all GS types reduced

the SRP peak concentrations (Dunnett's test, $p < 0.005$). There was an overall significant effect of the GS type, the release of P was lower for the high Fe_{ox} GS (GS2 and GS3) than for the low Fe_{ox} GS1. The 10% GS2 and 10% GS3 amendment consistently lowered the SRP concentration below the environmental threshold of 0.14 mg L^{-1}. In the second phase with GLU addition (Fig. 2), the SRP concentration in the control peaked above that of the first phase, illustrating more pronounced hypoxic conditions due to GLU addition. There was an effect of GS on P immobilisation, however the effects were smaller compared to the first phase without GLU addition and the order of effects reverted compared to the first phase, i.e., the SRP peak concentration decreased as GS1 > GS2 > GS3. Only the 5% GS1 significantly reduced P release compared to the control (Dunnett's test, $p < 0.05$) and neither GS type nor dose affected the peak SRP concentration (two-way ANOVA, $p > 0.05$).

The soluble P concentration in the pore waters were measured at day 22, i.e., after GLU additions. In the top 1cm GS amended layer, the average P concentration decreased from 7.5 ± 3.0 mg P L^{-1} in the control, to 4.7 ± 1.5 mg P L^{-1} in the 10% GS2 treatment and to 2.7 ± 1.7 mg P L^{-1} in the 10% GS3 treatment; the low Fe_{ox} GS1 did not significantly reduce pore water P ($p > 0.05$, Fig. 3a). The effects of GS on P concentration were also found in the unamend deeper layer, where the average P concentration decreased from 13.3 ± 2.1 mg P L^{-1} in the control, to 9.8 ± 3.4 mg P L^{-1} in the 10% GS2 treatment and to 6.1 ± 2.4 mg P L^{-1} in the 10% GS3 treatment. The GS amendments also reduced DGT labile P concentration in the sediment, but only in the amended layer (Fig. 3b). The DGT labile P concentration in the top 1 cm amended layer was reduced from 1.4 ± 0.6 mg P L^{-1} in the control to 0.9 ± 0.1 mg P L^{-1} by 10% GS2, 0.8 ± 0.5 mg P L^{-1} by 10% GS1 and 0.6 ± 0.4 mg P L^{-1} by 10% GS3.

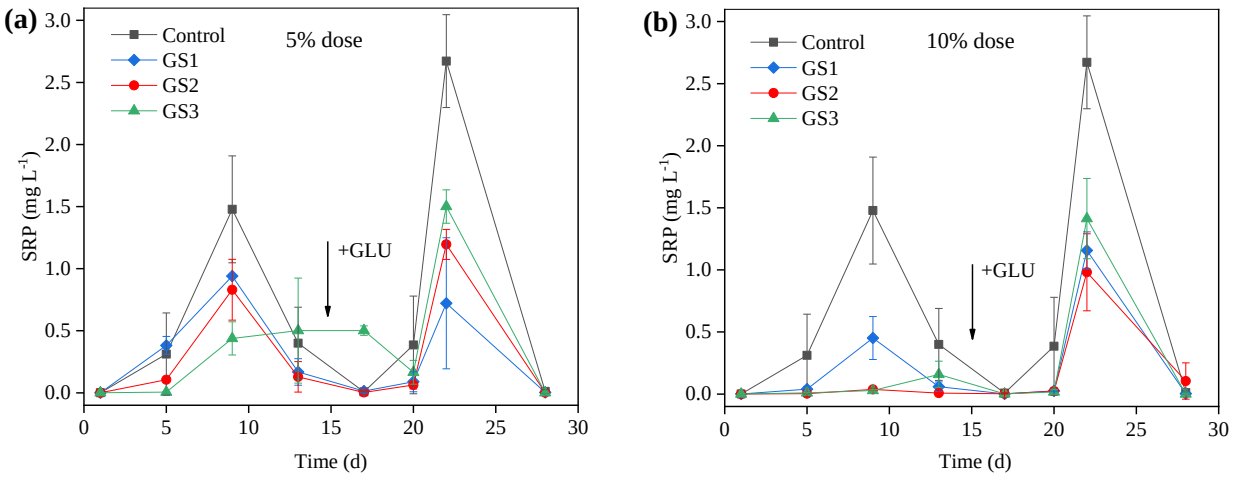

Fig. 2. Changes of soluble reactive P (SRP) in overlying water in the control and glauconite sand (GS) treatments under 5% dose (a) and 10% dose (b) during two phases of incubation. GS was added in the 10 mm surface layer and glutamate (GLU) was added to solutions at day 15 to stimulate strict anaerobic conditions. Error bars denote standard error of the means (n = 2, except for control, n = 3).

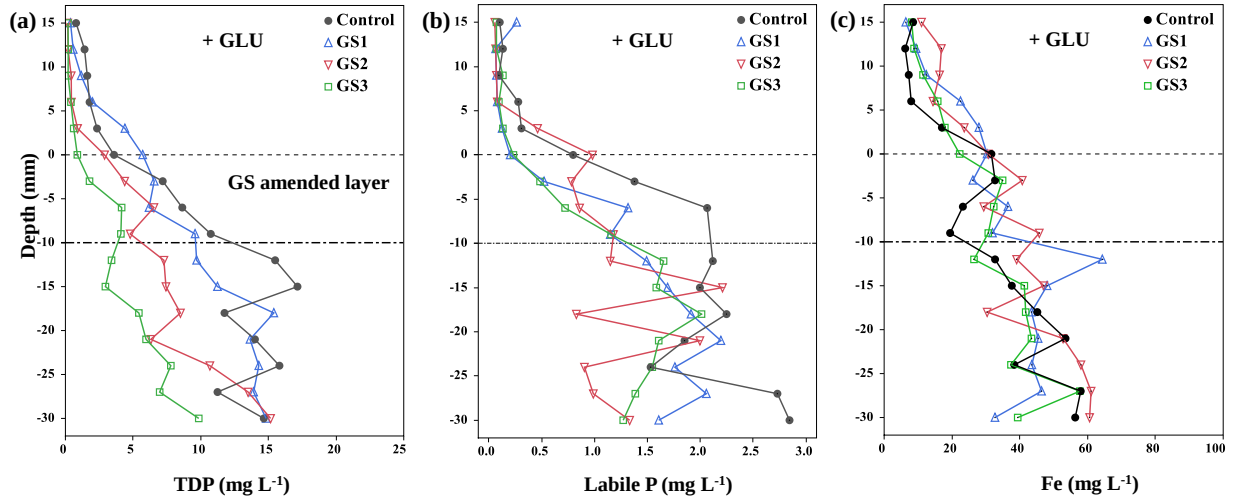

Fig. 3. Total dissolved P (TDP) and Fe measured by DET (a, c) and labile P measured by DGT (b) across the water/sediment interface (SWI) in the control and 10% (w/w) glauconite sand (GS) amended treatments at day 22 after glutamate (GLU) addition. The location of SWI is represented by zero and GS was added in the 10 mm surface layer.

3.3 The effect of GS amendment and GLU addition on Fe release

The dynamics of Fe release throughout the incubation followed the same trend as that of SRP and the P and Fe peaks coincided in time (Fig. 4). In the first phase without GLU addition, no significant difference in Fe concentration was found between the control, all 5% GS treatments or the 10% GS1 treatment (Dunnett's test, $p > 0.05$ for all). The Fe concentrations in these treatments peaked at about 8 mg L^{-1} at day 9. However, in the 10% GS2 and 10% GS3 treatments, i.e., at highest Fe_{ox} doses, less Fe was released (1.2 mg L^{-1}) than in the control. In the second phase with GLU addition, Fe concentrations were higher in all treatments than in the first phase and the peak Fe concentrations were higher for the high Fe_{ox} doses of GS2 and GS3 than for GS1, i.e., opposite to that in the first phase.

The difference in Fe concentration in the pore water among treatments was less pronounced than that in the overlying water (Fig. 3c). A general linear regression model showed that only the 10% GS2 treatment yielded higher Fe concentration than the control ($p<0.05$), the other treatments (GS1 and GS3) had similar Fe profiles as the control, with dissolved Fe up to 50 mg L^{-1}.

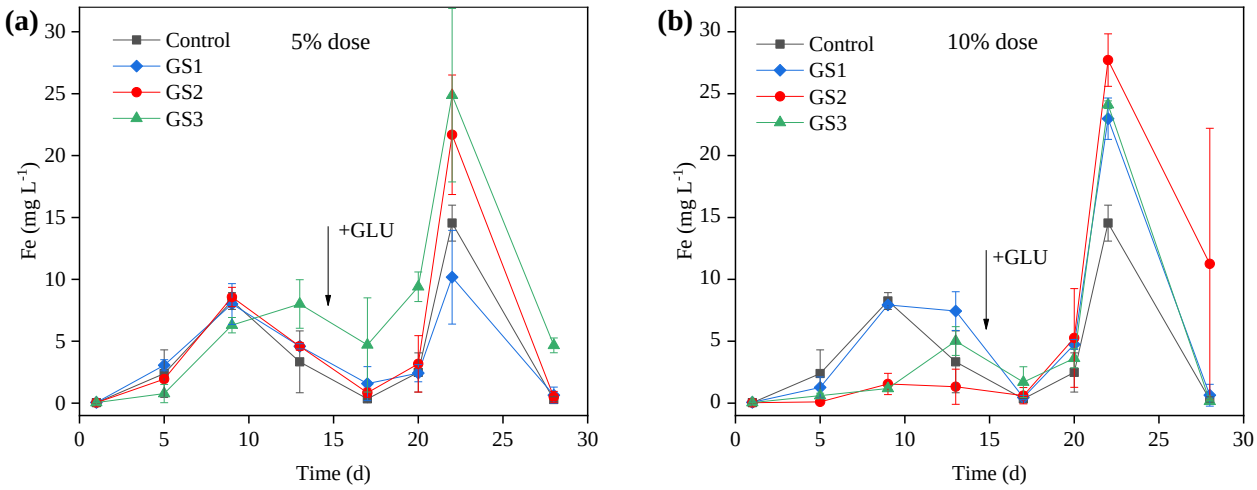

Fig. 4. Changes of Fe concentration in overlying water in the control and glauconite sand (GS) treatments under 5% dose (a) and 10% dose (b) during two phases of incubation. GS was added in the 10 mm surface layer and glutamate (GLU) was added to solutions at day 15 to stimulate strict anaerobic conditions. Error bars denote standard error of the means (n = 2, except for control, n = 3).

3.4 pH and DO profiles in the overlying water

The pH in the overlying water of the control sediment was 6.8 (Table S2) and was not different from that in all GS treatments (Dunnett's test, $p > 0.05$). The DO concentration in the control fluctuated between 2 and 4 mg L^{-1} until 0.3 cm above the SWI, then decreased to 0.6 mg L^{-1} at the SWI (Fig. 5). The DO changes over depth were different in GS treatments, where the DO concentration fluctuated between 4 and 6 mg L^{-1} until 2 cm above the SWI, then decreased to < 0.1 mg L^{-1}.

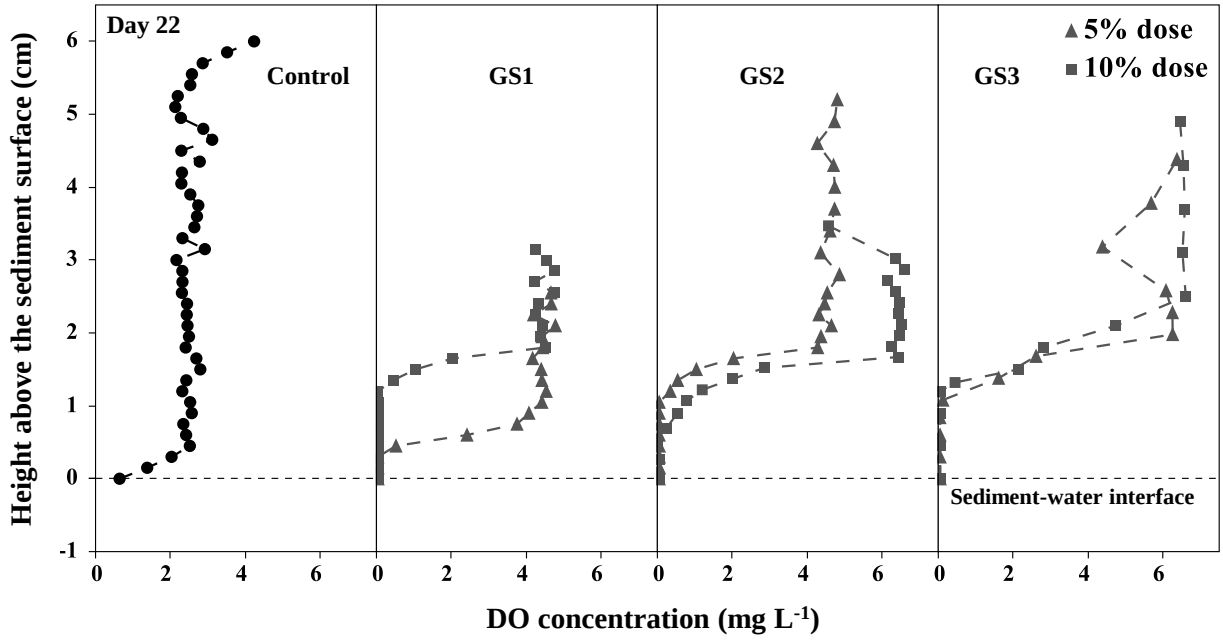

Fig. 5. Depth profile of the dissolved oxygen (DO) concentration in the overlying water under different sediment treatments with three different glauconite sands (GS). The profile was taken after 22 days. The horizontal dashed line is the sediment-water interface.

3.5 Changes in sediment P/Fe ratio after treatment

The sediment was collected at the end of the incubation. The bulk sediment, i.e., below the layer of GS and sediment mixture (< 1 cm depth), exhibited similar P/Fe ratios in all GS treatments (only evaluated for 10% dose) as in the control (Dunnett's test, $p > 0.05$), and these ratios were not significantly changed compared to that before the incubation (Table 1). In contrast, that ratio was affected in the surface layer of the sediment by time and treatment. In the unamended control sediment, the P/Fe decreased from 0.32 initially to 0.27

after incubation, largely because the Fe increased without changes in P concentration. Smaller P/Fe ratios were found in 10% GS1 (0.21) (Dunnett's test, $p < 0.01$) and 10% GS2 amended sediment (0.21) (Dunnett's test, $p < 0.01$), compared to the control, these values were also smaller than initial values (Table 1). However, no difference in P/Fe in surface sediment was found between the control and GS3 (Dunnett's test, $p > 0.05$).

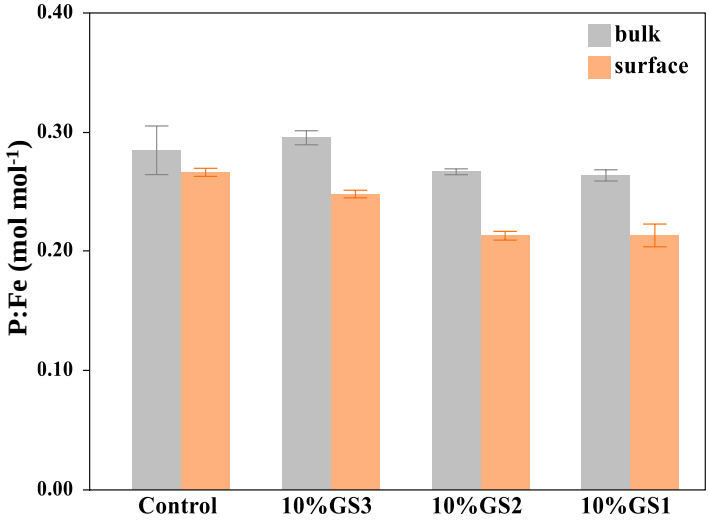

Fig. 6. The molar ratio of P and Fe in the sediment after 28 days incubation as affected by of the addition glauconite sand (GS). Surface samples are in the top 1 cm layer where the GS was mixed with sediment, bulk samples are below the layer of GS and sediment mixture (< 1 cm depth). Error bars denote standard error of the means (n = 2, except for control, n = 3).

3.6 Properties affecting the P immobilisation efficiency

The P and Fe concentrations were plotted (Fig. S3) and illustrate the contrasting treatment effects depending on type of GS and under the conditions without or with GLU. The P and Fe concentrations were given in millimole to compare P/Fe ratio in solution with P/Fe ratio in sediment. The molar P/Fe ratio of the dissolved fraction in the control (0.33) was close to that of the sediment (0.32, Table 1). In contrast, the pronounced mobilization of up to 0.5 mM Fe in GS amended sediment at day 22 did not coincide with such a release of SRP. The correlations between the GS characteristics and solution concentration were calculated to identify major factors affecting P immobilisation. Instead of using P concentration, the P immobilisation efficiency (SRP decrease as % of control SRP, Table S3) was used for correlation analysis

(Table 2). Before GLU addition, SRP immobilisation was positively correlated with adsorption capacity of GS and the doses of Fe and Al, either as total or as oxalate extractable contents, but was negatively correlated with theoretical P/Fe ratio in sediment. However, after GLU addition, no correlation was found between P immobilisation efficiency and GS dose or characteristics. The Fe peak was negatively correlated with added Fe_{ox}, but positively corelated with theoretical P/Fe ratio in sediment in the first phase without GLU addition, but opposite correlations were found in the second phase with GLU addition, for both Fe peak with added Fe_{ox} (r = 0.59), and Fe peak with P/Fe (r = -0.62).

4. Discussion

In this study, we first evaluated the P sorption capacity of three GS under oxic conditions. The estimated P sorption capacity of GS was lower than that of several solid P sorbents which are mainly synthesized materials (Table S4), such as Phoslock® (Mucci et al., 2018), dried amorphous ferric hydroxide (CFH-12®, Fuchs et al., 2018). However, they are still comparable with the values reported for natural minerals and for iron-modified zeolite (Table S4).

The three GS were subsequently amended to sediment and incubated to evaluate their P immobilisation ability under hypoxic conditions. The sediment molar P/Fe ratio was 0.32 before incubation (Table 1), suggesting that P release from the selected sediment was very likely to occur under hypoxic conditions (Jensen et al., 1992; Smolders et al., 2017). Indeed, the unamended sediment released up to 1.5 mg P L^{-1} under natural reducing conditions and to 2.7 mg P L^{-1} under GLU-stimulated conditions (Fig. 2). The P release under hypoxic conditions was mainly attributed to the reductive dissolution of Fe (oxy)hydroxides (Fig. 7a), i.e., the P release was strongly correlated to Fe release in both natural as well as GLU-stimulated conditions (Fig. S3). Then the P decreased after these peaks (Fig. 2), a trend that was found in similar static incubations (Smolders et al., 2017; van Dael et al., 2020b). For Fe the same trend was observed as for P (Fig. 4). Most likely, the anoxia in the sediment induces reductive dissolution of Fe, then Fe is transported by diffusion from the sediment to the water column where it is gradually oxidized and precipitated because the overlying water contains DO (Fig. 5). This can be also confirmed by the lower P/Fe ratio in the surface

sample after experiment compared to that in the deeper sediments (Fig. 6). This means that diffusion of Fe(II) from the deeper layer towards the surface contributed to Fe accumulation. Therefore, the decrease in P and Fe after their peak concentrations is explained by P precipitating with Fe(III) after re-oxidation of Fe(II) above the sediment-water interface (Smolders et al., 2017). That precipitation was also evidenced from the sediment surface layer that turned reddish during incubation, which was more pronounced in GS-treated sediments.

Table 2. The correlation coefficients between the P immobilisation efficiency (*IE*, %) or Fe concentration in the overlying water (Fe_w, mg L^{-1}) and properties of the glauconite sand and its mixtures in the sediment. The IE (Eq. 5) is the fraction of soluble reactive P of the unamended control that is immobilised by GS addition at day 9 (-GLU) or at day 22 (+GLU). Significant correlations are in bold, ***$p < 0.001$, **$p < 0.01$, *$p < 0.05$). Δ is the added amount (mg/pot) of each element that is calculated based on the properties of three GS (Table 1) and their corresponding doses, the molar P/Fe ratio (Eq. 2) is calculated from the nominal concentration in GS and sediment before mixing.

			Aqua regia			Oxalate extraction			
	Q_{max}	K_L	ΔFe	ΔAl	ΔMn	ΔFe	ΔAl	ΔMn	P/Fe
	mg/pot	L mg^{-1}	mg/pot	mg/pot	mg/pot	mg/pot	mg/pot	mg/pot	mol mol^{-1}
-GLU									
IE	**0.77****	0.15	**0.73****	**0.75****	0.54	**0.80****	**0.75****	0.56	**-0.76****
Fe_w	**-0.73****	-0.23	**-0.72****	**-0.72****	-0.54	**-0.89*****	**-0.69***	-0.55	**0.85*****
+GLU									
IE	-0.45	0.02	-0.50	-0.47	-0.50	-0.41	-042	-0.53	0.39
Fe_w	0.41	0.41	0.40	0.40	0.24	**0.59***	0.39	0.24	**-0.62***

Amending these Fe rich GS to sediments was successful in decreasing P peaks under natural reducing and GLU-stimulated conditions (Fig. 2), confirming what was found in a flume experiment (Van Dael et al., 2021). Under natural reducing conditions, higher Fe/Al addition and lower P/Fe ratio in the GS-treated sediment explained the lower P release and higher immobilisation efficiency (Table 2). The P released in the sediment was bound to the added Al oxides or residual Fe(III) oxides from the addition (Fig. 7b**,** Jensen et al., 1992; Smolders et al., 2001). The high P immobilisation efficiency achieved by 10% dose of GS (Table S3) is comparable to that obtained by some other P sorbents, such as iron-modified zeolite (72.2%–92.1%) when it was added to sediment at 10% dose (Zhan et al., 2019); drinking water treatment residuals (WTR, 85%) when added at 10% dry weight base (Wang et al., 2013b); magnetic microparticles (MMPs, 68% under oxic condition and 80% under anoxic condition) when added at MMPs: mobile P ratio of 85:1 (Funes et al., 2017). However, the 5% dose of GS was not enough to reduce internal loading, with lower P immobilisation efficiency of 36%-70% (Table S3), compared to 10% dose of GS and other P sorbents. In addition, the soluble Fe was lower in 10% GS treated sediments than in the control sediment (Fig. 4b). The occurrence of lower Fe release from the high Fe-dosed treatments (Fig. S3) was probably related to a combination of mechanisms. First, a higher Fe dose could yield more Fe(II) during hypoxic conditions (< 2 mg DO L^{-1}) that would migrate to the SWI where it is faster precipitated as Fe(III)(oxy)hydroxides, without yielding dissolved forms in overlying water. This creates a high Fe and P local layer on the surface of high Fe-dosed sediment, and that formation could be enhanced when more Fe(II) was diffusing to the SWI because of a higher saturation index of possible precipitates. Second, enhanced GS addition could also enhance the adsorption of Fe^{2+} by cation exchange or adsorption to the residual or freshly precipitated Fe oxides or to Al oxides. Similar effects of CEC on Fe concentration had also been found for Al modified clay (Wang et al., 2019) and La modified bentonite (Ding et al., 2018) where lower Fe concentrations were found in treated sediment cores. Overall, the coincidence of the low solution P and Fe in GS treated sediments was attributed to a local Fe(II)/Fe(III)-P (oxy)hydroxides layer formed on the sediment surface. However, when GS was exposed to high loading of GLU, neither dose nor GS type were important for reducing the P peaks, although the application of GS still reduced internal P loading, compared to the

control sediment. The higher P and Fe release in higher Fe-dose sediments, compared to lower Fe-dose treatments suggests that the previously trapped P by GS was released (**Fig. 7c)**. This could have far reaching consequences on the longevity of this practice in the field. However, it should be noted that the dose of GLU was high: a dose equivalent to a BOD of 50 mg O_2 L^{-1} during high temperatures was unusual (Baetens, 2016). For example, the P90 of BOD_5 concentrations in lowland rivers was only 10 mg O_2 L^{-1}. Therefore, the application of GS is best accompanied by measures to avoid high loading of organic matter, for example, by further reducing the BOD in effluents through deep wastewater treatments.

The glauconite sands are abundantly available and are an unused by-product generated during exploitation of quartz sands. Thus, using GS as amendment does not only keep the costs down, but also allows the valorisation of rest streams from construction (excavation) works. In addition, GS has the benefit of being non-toxic. The GS amended to the sediments did not significantly release toxic trace metals, with maximum concentrations of 0.2 µg Cr L^{-1}, 0.4 µg Cu L^{-1}, 1.8 µg Ni L^{-1}, 0.3 µg Pb L^{-1} and 3.2 µg Zn L^{-1}. All metals were below their predicted no effect concentrations (PNEC) in freshwaters according to the European Chemicals Agency (ECHA). Therefore, our results indicate that GS could be a feasible P sorbent to tackle internal loading. However, it should be emphasized that the performance of GS was not tested under longer period of hypoxic conditions, thus, more tests on the efficacy and longevity of GS under seasonal hypoxia should be conducted before large application.

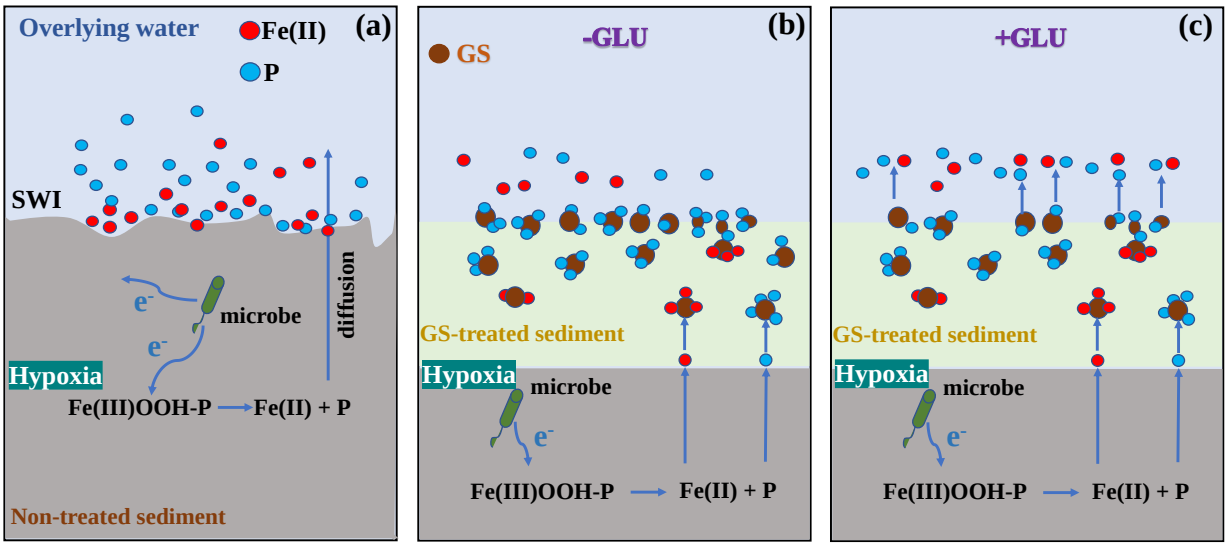

Fig. 7. The scheme of P release in different treatments: P release from sediment in the control under hypoxic conditions (a); the P released in the sediment is bound to the added Al oxides or residual Fe(III) oxides from the glauconite sand (GS) (b); the P adsorbed on GS is partially released when residual DO at SWI was depleted by adding glutamate (+GLU) (c).

5. Conclusions

In this study, the P release from the sediment amended with three different GS at two doses were compared to identify dose and GS property dependent P immobilisation in the sediment. Sediment incubations under hypoxic conditions showed that the GS could effectively reduce P concentration both in the pore water and overlying water, and the immobilisation efficiency was related to the sorption capacity of GS and its Fe and Al contents. GS with higher Fe/Al content and higher dose had higher effects on P immobilisation. Therefore, the characteristics of GS including oxalate extractable and total content of Fe and Al should be considered when selecting these as P sorbents. The effect of extreme high BOD concentrations on GS efficacy in trapping P should be further explored in order to estimate longevity of application.

CRediT authorship contribution statement

Lei Xia: Conceptualization, Methodology, Validation, Formal analysis, Investigation, Writing-original draft, Writing-review & editing, Visualization. **Tom David**: Investigation, Formal analysis. **Mieke**

Verbeeck: Conceptualization, Writing-review & editing, Supervision. **Yaana Bruneel**: Resources, Writing-review & editing. **Erik Smolders**: Conceptualization, Resources, Writing-review & editing, Supervision.

Acknowledgements

We would like to thank the P team of KU Leuven for useful discussions regarding the data interpretation. We also thank the ICP team for the ICP measurements. We are grateful to the China Scholarship Council (No.201808510179) for granting a PhD fellowship to the corresponding author. We thank Yan Zhao (Department of Chemical Engineering, KU Leuven) for his suggestions and modifications on the manuscript that improved the manuscript.

References

Baetens, E., 2016. Seasonal fluctuations of phosphate in Flemish streams: the impact of iron concentrations in the sediment 68.

Baken, S., Verbeeck, M., Verheyen, D., Diels, J., Smolders, E., 2015. Phosphorus losses from agricultural land to natural waters are reduced by immobilization in iron-rich sediments of drainage ditches. Water Res. 71, 160–170. https://doi.org/10.1016/j.watres.2015.01.008

Bruneel, Y., Van Laer, L., Brassinnes, S., Smolders, E., 2021. Radiostrontium sorption on natural glauconite sands of the Neogene-Paleogene formations in Belgium. J. Environ. Radioact. 233, 1–9. https://doi.org/10.1016/j.jenvrad.2021.106588

Bruneel, Y., Van Laer, L., Brassinnes, S., Smolders, E., 2020. Radiocaesium sorption on natural glauconite sands is unexpectedly as strong as on Boom Clay. Sci. Total Environ. 720, 137392. https://doi.org/10.1016/j.scitotenv.2020.137392

Chen, J., Yan, L.G., Yu, H.Q., Li, S., Qin, L.L., Liu, G.Q., Li, Y.F., Du, B., 2016. Efficient removal of phosphate by facile prepared magnetic diatomite and illite clay from aqueous solution. Chem. Eng. J. 287, 162–172. https://doi.org/10.1016/j.cej.2015.11.028

Copetti, D., Finsterle, K., Marziali, L., Stefani, F., Tartari, G., Douglas, G., Reitzel, K., Spears, B.M.,

Winfield, I.J., Crosa, G., D'Haese, P., Yasseri, S., Lürling, M., 2015. Eutrophication management in surface waters using lanthanum modified bentonite: A review. Water Res. 97, 162–174. https://doi.org/10.1016/j.watres.2015.11.056

Davison, W., Grimet, G.W., Morgan, J.A.W., Clarke, K., 1991. Davison et al, 1991 Distribution of dissolved iron in sediment pore waters at submillimetre resolution.pdf.

Ding, S., Sun, Q., Chen, X., Liu, Q., Wang, D., Lin, J., Zhang, C., Tsang, D.C.W., 2018. Synergistic adsorption of phosphorus by iron in lanthanum modified bentonite (Phoslock®): New insight into sediment phosphorus immobilization. Water Res. 134, 32–43. https://doi.org/10.1016/j.watres.2018.01.055

ECHA, n.d. Registration Dossier of Cr, Cu, Ni Pb and Zn [WWW Document]. URL echa.europe.eu

Fuchs, E., Funes, A., Saar, K., Reitzel, K., Jensen, H.S., 2018. Evaluation of dried amorphous ferric hydroxide CFH-12® as agent for binding bioavailable phosphorus in lake sediments. Sci. Total Environ. 628–629, 990–996. https://doi.org/10.1016/j.scitotenv.2018.02.059

Funes, A., del Arco, A., Álvarez-Manzaneda, I., de Vicente, J., de Vicente, I., 2017. A microcosm experiment to determine the consequences of magnetic microparticles application on water quality and sediment phosphorus pools. Sci. Total Environ. 579, 245–253. https://doi.org/10.1016/j.scitotenv.2016.11.120

Funes, A., Martínez, F.J., Álvarez-Manzaneda, I., Conde-Porcuna, J.M., de Vicente, J., Guerrero, F., de Vicente, I., 2018. Determining major factors controlling phosphorus removal by promising adsorbents used for lake restoration: A linear mixed model approach. Water Res. 141, 377–386. https://doi.org/10.1016/j.watres.2018.05.029

Gibbs, M.M., Hickey, C.W., Özkundakci, D., 2011. Sustainability assessment and comparison of efficacy of four P-inactivation agents for managing internal phosphorus loads in lakes: Sediment incubations. Hydrobiologia 658, 253–275. https://doi.org/10.1007/s10750-010-0477-3

Guan, D., Williams, P.N., Luo, J., Zheng, J., Xu, H., Cai, C., Ma, L.Q., 2015. Novel Precipitated Zirconia-Based DGT Technique for High- Resolution Imaging of Oxyanions in Waters and

Sediments. Environ. Sci. Technol. 49, 3653–3661. https://doi.org/10.1021/es505424m

Heinrich, L., Rothe, M., Braun, B., Hupfer, M., 2021. Transformation of redox-sensitive to redox-stable iron-bound phosphorus in anoxic lake sediments under laboratory conditions. Water Res. 189, 116609. https://doi.org/10.1016/J.WATRES.2020.116609

Huser, B.J., Futter, M., Lee, J.T., Perniel, M., 2016. In-lake measures for phosphorus control: The most feasible and cost-effective solution for long-term management of water quality in urban lakes. Water Res. 97, 142–152. https://doi.org/10.1016/j.watres.2015.07.036

Jensen, H.S., Kristensen, P., Jeppesen, E., Skytthe, A., 1992. Iron:phosphorus ratio in surface sediment as an indicator of phosphate release from aerobic sediments in shallow lakes. Hydrobiologia 235–236, 731–743. https://doi.org/10.1007/BF00026261

Jensen, H.S., Reitzel, K., Egemose, S., 2015. Evaluation of aluminum treatment efficiency on water quality and internal phosphorus cycling in six Danish lakes. Hydrobiologia 751, 189–199. https://doi.org/10.1007/s10750-015-2186-4

Kleeberg, A., Herzog, C., Hupfer, M., 2013. Redox sensitivity of iron in phosphorus binding does not impede lake restoration. Water Res. 47, 1491–1502. https://doi.org/10.1016/j.watres.2012.12.014

Liu, T., Wang, H., Zhang, Z., Zhao, D., 2017. Application of synthetic iron-oxide coated zeolite for the pollution control of river sediments. Chemosphere 180, 160–168. https://doi.org/10.1016/j.chemosphere.2017.04.023

Lyngsie, G., Borggaard, O.K., Hansen, H.C.B., 2014. A three-step test of phosphate sorption efficiency of potential agricultural drainage filter materials. Water Res. 51, 256–265. https://doi.org/10.1016/j.watres.2013.10.061

Mucci, M., Maliaka, V., Noyma, N.P., Marinho, M.M., Lürling, M., 2018. Assessment of possible solid-phase phosphate sorbents to mitigate eutrophication: Influence of pH and anoxia. Sci. Total Environ. 619–620, 1431–1440. https://doi.org/10.1016/j.scitotenv.2017.11.198

Murphy, J., Riley, J.P., 1962. DETERMrNATION SINGLE SOLUTION METHOD FOR THE IN NATURAL. Anal. Chim. Acta 27, 31–36.

Schwertmann, U., 1964. Solubility and dissolution of iron-oxides. Plant Soil 130, 1–25. https://doi.org/10.1007/BF00011851   Published: JAN 1991

Smolders, A.J.P., Lamers, L.P.M., Moonen, M., Zwaga, K., Roelofs, J.G.M., 2001. Controlling phosphate release from phosphate-enriched sediments by adding various iron compounds. Biogeochemistry 54, 219–228. https://doi.org/10.1023/A:1010660401527

Smolders, E., Baetens, E., Verbeeck, M., Nawara, S., Diels, J., Verdievel, M., Peeters, B., De Cooman, W., Baken, S., 2017. Internal Loading and Redox Cycling of Sediment Iron Explain Reactive Phosphorus Concentrations in Lowland Rivers. Environ. Sci. Technol. 51, 2584–2592. https://doi.org/10.1021/acs.est.6b04337

Spears, B.M., Maberly, S.C., Pan, G., Mackay, E., Bruere, A., Corker, N., Douglas, G., Egemose, S., Hamilton, D., Hatton-Ellis, T., Huser, B., Li, W., Meis, S., Moss, B., Lürling, M., Phillips, G., Yasseri, S., Reitzel, K., 2014. Geo-engineering in lakes: A crisis of confidence? Environ. Sci. Technol. 48, 9977–9979. https://doi.org/10.1021/es5036267

van Dael, T., De Cooman, T., Smolders, E., 2020a. In-stream oxygenation to mitigate internal loading of phosphorus in lowland streams. J. Hydrol. 590, 125536. https://doi.org/10.1016/j.jhydrol.2020.125536

van Dael, T., De Cooman, T., Verbeeck, M., Smolders, E., 2020b. Sediment respiration contributes to phosphate release in lowland surface waters. Water Res. 168, 115168. https://doi.org/10.1016/j.watres.2019.115168

Van Dael, T., Xia, L., Van Dijck, K., Potemans, S., Smolders, E., 2021. Internal loading of phosphate in rivers reduces at higher flow velocity and is reduced by iron rich sand application: an experimental study in flumes. Water Res. 198, 117160. https://doi.org/10.1016/j.watres.2021.117160

Voegelin, A., Senn, A.C., Kaegi, R., Hug, S.J., Mangold, S., 2013. Dynamic Fe-precipitate formation induced by Fe(II) oxidation in aerated phosphate-containing water. Geochim. Cosmochim. Acta 117, 216–231. https://doi.org/10.1016/j.gca.2013.04.022

Wang, C., Bai, L., Pei, Y., 2013a. Assessing the stability of phosphorus in lake sediments amended with

water treatment residuals. J. Environ. Manage. 122, 31–36. https://doi.org/10.1016/j.jenvman.2013.03.007

Wang, C., Gao, S., Pei, Y., Zhao, Y., 2013b. Use of drinking water treatment residuals to control the internal phosphorus loading from lake sediments: Laboratory scale investigation. Chem. Eng. J. 225, 93–99. https://doi.org/10.1016/j.cej.2013.03.074

Wang, C., Liang, J., Pei, Y., Wendling, L.A., 2013c. A method for determining the treatment dosage of drinking water treatment residuals for effective phosphorus immobilization in sediments. Ecol. Eng. 60, 421–427. https://doi.org/10.1016/j.ecoleng.2013.09.045

Wang, J., Chen, J., Chen, Q., Yang, H., Zeng, Y., Yu, P., Jin, Z., 2019. Assessment on the effects of aluminum-modified clay in inactivating internal phosphorus in deep eutrophic reservoirs. Chemosphere 215, 657–667. https://doi.org/10.1016/j.chemosphere.2018.10.095

Wang, Q., Liao, Z., Yao, D., Yang, Z., Wu, Y., Tang, C., 2021. Phosphorus immobilization in water and sediment using iron-based materials: A review. Sci. Total Environ. 767, 144246. https://doi.org/10.1016/j.scitotenv.2020.144246

Yin, H., Kong, M., Fan, C., 2013. Batch investigations on P immobilization from wastewaters and sediment using natural calcium rich sepiolite as a reactive material. Water Res. 47, 4247–4258. https://doi.org/10.1016/j.watres.2013.04.044

Zhan, Y., Yu, Y., Lin, J., Wu, X., Wang, Y., Zhao, Y., 2019. Simultaneous control of nitrogen and phosphorus release from sediments using iron-modified zeolite as capping and amendment materials. J. Environ. Manage. 249. https://doi.org/10.1016/j.jenvman.2019.109369

Zou, Y., Grace, M.R., Roberts, K.L., Yu, X., 2017. Thin ferrihydrite sediment capping sequestrates phosphorus experiencing redox conditions in a shallow temperate lacustrine wetland. Chemosphere 185, 673–680. https://doi.org/10.1016/j.chemosphere.2017.07.052

Supporting information

Iron rich glauconite sand as an efficient phosphate immobilising agent in river sediments

Lei Xia [a,*], Tom David [a], Mieke Verbeeck [b], Yaana Bruneel [c], Erik Smolders [a]

[a] Division of Soil and Water Management, Department of Earth and Environmental Sciences, KU Leuven, Kasteelpark Arenberg 20 bus 2459, 3001 Leuven, Belgium.

[b] Rothamsted Research, Sustainable Agriculture Sciences, North Wyke, EX20 2SB, UK.

[c] Laboratoire de Mesure et Modélisation de la Migration des Radionucléides (L3MR), CEA Commissariat à l'énergie atomique et aux énergies alternatives, Paris-Saclay, France

*Corresponding author: E-mail: lei.xia@kuleuven.be

Fig. S1. Light microscopy images of glauconite fraction of GS from Lubbeek. Glauconite pellets showing signs of strong oxidation, with Fe (oxy)hydroxides coating on the glauconite, as well as on the quartz grains (right in the 2nd row).

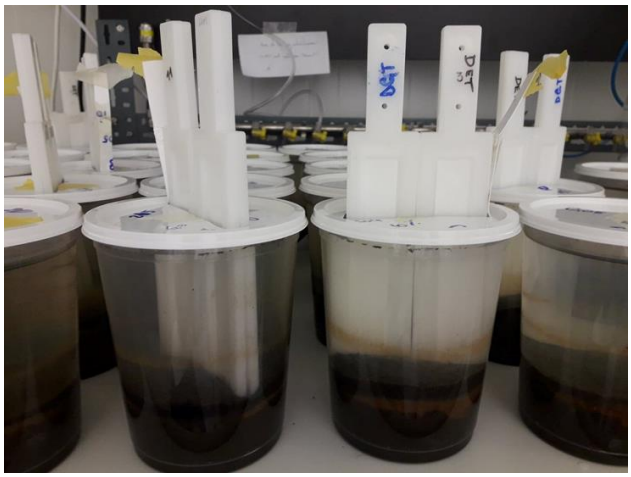

Fig. S2. The deployment of DET and DGT probes in the sediment.

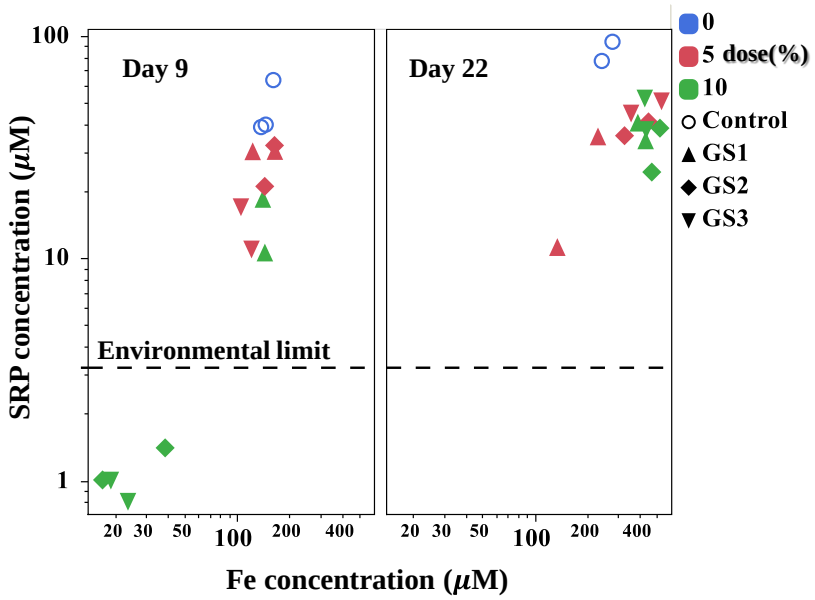

Fig. S3. The relationship between the SRP and Fe concentrations in the overlying water (both are log scale) at day 9 without GLU addition and at day 22 with GLU addition. The dashed line indicates the P environmental limit at 3.2 μM.

Table S1. Theoretical molar ratio of P/Fe of the top 1 cm sediment layer after GS amendment.

Sediment/GS mixture	Control	GS1		GS2		GS3	
		5%	10%	5%	10%	5%	10%
	0.32	0.32	0.32	0.29	0.26	0.28	0.25

Table S2. The pH in the overlying water (means ± standard deviation) at day 22.

Treatment	Control	GS1		GS2		GS3	
		5%	10%	5%	10%	5%	10%
pH	6.8 ± 0.0	6.8 ± 0.0	6.8 ± 0.3	6.8 ± 0.1	6.8 ± 0.1	6.7 ± 0.1	6.8 ± 0.1

Table S3. The IE (%, means ± standard deviation) by GS amendment at day 9 before GLU addition and at day 22 after GLU addition. The IE was calculated by Eq. 5.

Treatment	P immobilisation efficiency (%)	
	Day 9 (+GLU)	Day 22 (+GLU)
5% GS1	36.4 ± 0.1	73.0 ± 19.8
10% GS1	69.5 ± 11.7	56.7 ± 5.6
5% GS2	43.8 ± 16.6	55.2 ± 4.5
10% GS2	97.5 ± 0.6	63.3 ± 11.6
5% GS3	70.3 ± 9.1	43.9 ± 5.1
10% GS3	98.1 ± 0.3	47.1 ± 12.1

Table S4. Comparison of phosphate adsorption capacity for different solid P sorbents

Solid P sorbents	Q_m (mg P/kg)	Reference
Glauconite sands	590-1230	This study
Bentonite	1607	Gu et al., 2019
Illite	3296	Gu et al., 2019
Zeolite	500-2000	Wendling et al., 2013
Red soil	300-2900	Mucci et al., 2018; Noyma et al., 2016
Iron-coated sand (ICS)	10510	Vandermoere et al., 2018
Bauxite	3400	Mucci et al., 2018
Steel slag	2000	Drizo et al., 2006
drinking water treatment residuals (WTRs)	3000-8000	Bai et al., 2014
Iron-modified zeolite	506-966	Liu et al., 2017; Zhan et al., 2019
Phoslock®	2380-11000	Mucci et al., 2018
CFH-12®	15100	Funes et al., 2018

References

Bai, L., Wang, C., He, L., Pei, Y., 2014. Influence of the inherent properties of drinking water treatment residuals on their phosphorus adsorption capacities. J. Environ. Sci. (China) 26, 2397–2405. https://doi.org/10.1016/j.jes.2014.04.002

Drizo, A., Forget, C., Chapuis, R.P., Comeau, Y., 2006. Phosphorus removal by electric arc furnace steel slag and serpentinite. Water Res. 40, 1547–1554. https://doi.org/10.1016/J.WATRES.2006.02.001

Funes, A., Martínez, F.J., Álvarez-Manzaneda, I., Conde-Porcuna, J.M., de Vicente, J., Guerrero, F., de Vicente, I., 2018. Determining major factors controlling phosphorus removal by promising adsorbents used for lake restoration: A linear mixed model approach. Water Res. 141, 377–386. https://doi.org/10.1016/j.watres.2018.05.029

Gu, B.W., Hong, S.H., Lee, C.G., Park, S.J., 2019. The feasibility of using bentonite, illite, and zeolite as capping materials to stabilize nutrients and interrupt their release from contaminated lake sediments. Chemosphere 219, 217–226. https://doi.org/10.1016/j.chemosphere.2018.12.021

Liu, T., Wang, H., Zhang, Z., Zhao, D., 2017. Application of synthetic iron-oxide coated zeolite for the pollution control of river sediments. Chemosphere 180, 160–168. https://doi.org/10.1016/j.chemosphere.2017.04.023

Mucci, M., Maliaka, V., Noyma, N.P., Marinho, M.M., Lürling, M., 2018. Assessment of possible solid-phase phosphate sorbents to mitigate eutrophication: Influence of pH and anoxia. Sci. Total Environ. 619–620, 1431–1440. https://doi.org/10.1016/j.scitotenv.2017.11.198

Noyma, N.P., de Magalhães, L., Furtado, L.L., Mucci, M., van Oosterhout, F., Huszar, V.L.M., Marinho, M.M., Lürling, M., 2016. Controlling cyanobacterial blooms through effective flocculation and sedimentation with combined use of flocculants and phosphorus adsorbing natural soil and modified clay. Water Res. 97, 26–38. https://doi.org/10.1016/j.watres.2015.11.057

Vandermoere, S., Ralaizafisoloarivony, N.A., Van Ranst, E., De Neve, S., 2018. Reducing phosphorus (P) losses from drained agricultural fields with iron coated sand (- glauconite) filters. Water Res. 141, 329–339. https://doi.org/10.1016/j.watres.2018.05.022

Wendling, L.A., Blomberg, P., Sarlin, T., Priha, O., Arnold, M., 2013. Phosphorus sorption and recovery using mineral-based materials: Sorption mechanisms and potential phytoavailability. Appl. Geochemistry 37, 157–169. https://doi.org/10.1016/j.apgeochem.2013.07.016

Zhan, Y., Yu, Y., Lin, J., Wu, X., Wang, Y., Zhao, Y., 2019. Simultaneous control of nitrogen and phosphorus release from sediments using iron-modified zeolite as capping and amendment materials. J. Environ. Manage. 249. https://doi.org/10.1016/j.jenvman.2019.109369